Received: 6 October 2022 | Revised: 9 March 2023 | Accepted: 15 March 2023

DOI: 10.1002/pmic.202200408

RESEARCH ARTICLE

Proteomics
Proteomics and Systems Biology

DiaPASEF proteotype analysis indicates changes in cell growth and metabolic switch induced by caspase-9 inhibition in chondrogenic cells

Petr Lapcik[1] | Barbora Vesela[2] | David Potesil[3] | Katerina Dadakova[2] | Martina Zapletalova[2] | Petr Benes[4,5] | Pavel Bouchal[1] | Eva Matalova[2,6]

[1]Department of Biochemistry, Faculty of Science, Masaryk University, Brno, Czech Republic

[2]Laboratory of Odontogenesis and Osteogenesis, Institute of Animal Physiology and Genetics, Czech Academy of Sciences, Brno, Czech Republic

[3]Proteomics core facility, Central European Institute for Technology, Masaryk University, Brno, Czech Republic

[4]Department of Experimental Biology, Faculty of Science, Masaryk University, Brno, Czech Republic

[5]International Clinical Research Center, St. Anne's University Hospital, Brno, Czech Republic

[6]Department of Physiology, Faculty of Veterinary Medicine, Veterinary University, Brno, Czech Republic

Correspondence
Pavel Bouchal, Faculty of Science, Department of Biochemistry, Masaryk University, Kamenice 5, 62500 Brno, Czech Republic.
Email: bouchal@chemi.muni.cz

Petr Lapcik and Barbora Vesela contributed equally.

Abstract

Caspase-9 is the major apical caspase responsible for triggering the intrinsic apoptotic pathway. Our previous study indicated that specific inhibition of caspase-9 caused microscopically evident alterations in appearance of the primary chondrogenic cultures which cannot be explained by decrease in apoptosis. To describe a complex molecular background of this effect, proteomics analysis of control and caspase-9 inhibitor-treated chondrogenic cultures were performed. Proteins were extracted, identified and quantified using LC-MS in both data dependent and data independent acquisition (DIA) mode. While directDIA analysis of diaPASEF data obtained using timsTOF Pro LC-MS system revealed 7849 protein groups (Q-value <0.01), a parallel analysis of iTRAQ-2DLC-MS3 and conventional DIA-MS data identified only 5146 and 4098 protein groups, respectively, showing diaPASEF a superior method for the study. The detailed analysis of diaPASEF data disclosed 236/551 significantly down-/up-regulated protein groups after caspase-9 inhibition, respectively (|log2FC|>0.58, Q value <0.05). Classification of downregulated proteins revealed changes in extracellular matrix organization, collagen metabolism, and muscle system processes. Moreover, deregulations suggest a switch from glycolytic to lipid based metabolism in the inhibited cells. No essential changes were found in the proteins involved in apoptosis. The data indicate new non-apoptotic participation of caspases in chondrocyte homeostasis with potential applications in cartilage pathophysiology.

KEYWORDS
caspase-9, chondrogenesis, diaPASEF, micromass cultures, proteomics

1 | INTRODUCTION

Development of long bones by endochondral ossification is based on formation of bone tissue within a cartilage model. Later, chondrocytes located in the growth plate are critical for bone elongation. Recent lineage studies, supporting the presence of skeletal stem cells within cartilage make such research particularly challenging [1]. Growth plate chondrocytes are intensely investigated in basic research but also with respect to the spectrum of skeletal and metabolic disorders [2, 3]. Changes in chondrocyte behavior are associated also

with osteoarthritis [4, 5], rheumatoid arthritis [6], and increased chondrocyte proliferation without a change in apoptosis was reported in osteoporosis [7].

The signaling pathways in chondrocytes include particularly bone morphogenetic proteins (BMPs), SRY-related high-mobility group-box gene 9 (Sox9), parathyroid hormone-related peptide (PTHrP), Indian hedgehog (Ihh), fibroblast growth factor receptor 3 (FGFR3), and β-catenin [8]. Caspases, cysteine proteases, were investigated in chondrocytes mostly in association with their traditional roles in apoptosis and inflammation [9, 10] including pathogenesis of osteoarthritis [11], rheumatoid arthritis [12], or osteoporosis [13]. Notably, active caspases were found in the growth plate also during physiological endochondral ossification [14] and their appearance supported the increasing evidence about not yet unrevealed functions of caspases beyond apoptosis and inflammation [15].

Caspases are produced within cells as inactive zymogens and become activated upon extrinsic (receptor mediated) or intrinsic (mitochondria) triggering. Due to this fact, modulations of caspase cascade are performed at the protein level. The most common approach is application of inhibitors such as fluoromethylketone (FMK) [16]. These synthetic inhibitors bind to the active site of caspase and irreversibly block its activity, but do not affect the presence or detectability of caspase protein. So far, general caspase FMK inhibition in chondrogenic micromass cultures pointed to engagement of caspases in osteogenic [14, 17] and autophagic pathways [18]. Recently, general caspase inhibition in chondrocytic cultures led to modified expression of several osteoarthritis related genes [19]. In order to reveal impact of individual caspases on the expression profile in chondrocytes, specific inhibitors may be applied.

Caspase-9 is the major apical caspase of the intrinsic pathway initiated mostly from mitochondria. Activated caspase-9 was present in growth plate chondrocytes [14] and was also detected during chondrogenesis in vitro [20], where its inhibition affected gene expression of chondrogenesis-related genes.

In our investigation, specific inhibition of caspase-9 caused morphological changes in chondrogenic micromass cultures which could not be simply explained by modulation of apoptosis. To search for possible background of such changes, proteomics analysis using the DIA - Parallel Accumulation Serial Fragmentation (diaPASEF) approach on timsTOF Pro was designed to compare the profile subjected to FMK-caspase-9 inhibitor treatment and control cultures. The timsTOF Pro employs the Trapped Ion Mobility Spectrometer (TIMS) analyzer that allows separation of eluting precursor ions based on the ion mobility. This additional separation dimension decreases the complexity of MS/MS spectra, resulting in increased sensitivity of peptide identification [21]. The combination of PASEF with DIA mode further improves the quantification capabilities of the method as almost complete sampling of the precursor ions is achieved [21]. We moreover compared the diaPASEF method to widely used data-dependent acquisition (DDA) method with iTRAQ-8plex labeling together with conventional DIA method, both executed on orbitrap Lumos, and we demonstrate superiority of the diaPASEF in number of quantified peptides and protein groups. Using this approach, we uncovered changes of proteins involved in extracellular matrix organization, muscle system processes and in glycolytic and lipid metabolism after the caspase-9 inhibition.

Statement of significance of the study

Emerging non-apoptotic functions of caspases are one of the hot topics because of their significance in several pathologies. Such novel aspects have been recently reported in the bone and cartilage, for example, with respect to osteoarthritis. The role of individual caspases, however, remains to be specified. Inhibition of caspase-9, a key apical caspase, in chondrogenic cultures resulted in clear morphological alterations which cannot be explained by modification of apoptosis. To clarify the molecular mechanisms associated with caspase-9 inhibition, we applied three LC-MS/MS-based proteomics strategies, including diaPASEF, iTRAQ-2DLC-MS3, and conventional DIA, and demonstrated superior performance of the diaPASEF approach allowing deep quantification of the proteome.

Our results provide a complex insight into the background of the effect of capsase-9 inhibition and point to significant changes in extracellular matrix organization, particularly collagen metabolic processes. Additionally, a switch from glycolytic to lipid metabolism in chondrocytes treated by caspase-9 inhibitor was indicated. Caspase inhibitors and collagen-based treatment are considered in anti-osteoarthritic therapies and metabolic pathways in osteoarthritis become also intensely investigated.

2 | MATERIALS AND METHODS

2.1 | Micromass cultures

Cells for micromass cultures were obtained from fresh post mortem mouse forelimbs at embryonic day (E) 12. Each sample was prepared from biological material obtained from 4 to 6 prenatal mice. Limbs were cut in pieces and incubated 1–2 h in 37°C with Dispase (Gibco, final activity 1 U/mL). Cells at a concentration of 2×10^7/mL were spotted in 10 μL drops on the culture plate. Culture medium supporting chondrogenic differentiation was composed of DMEM (Sigma-Aldrich) and Nutrient Mixture F12 (Sigma-Aldrich) in proportion 2:3, 10 % FBS (Sigma Aldrich), penicillin/streptomycin (Sigma-Aldrich, final concertation 100 U/mL and 100 μg/mL), L-glutamine (Sigma-Aldrich, final concentration 2 mM), β-glycerol phosphate (Sigma-Aldrich, final concentration 10 mM), and ascorbic acid (Sigma-Aldrich, final concentration 50 μg/ml). Cell were cultured overnight in order to adhere to the surface. For caspase-9 inhibition, pharmacological inhibitor Z-LEHD-FMK (FMK008, R&D Systems) was applied to the micromass cultures at a concentration of 100 μM, according to the manufacturer's recommendation and previous studies [18]. In the controls, DMSO as an inhibitor

vehicle was added. The medium with caspase inhibitor or DMSO was changed every second day up to 7 days of cultivation. After this time, samples were collected for proteomic analysis. The experiments were performed in four biological replicates. For proteomics, cells were lysed in buffer containing 8 M urea in 0.5 M triethylammonium bicarbonate (TEAB), pH 8.5, sonicated (50 W, 30*0.1 s, then 30 s pause and 30*0.1 s) using needle sonication (Bandelin HD 2200; Bandelin, Germany) and incubated on ice for 75 min. Lysates were further centrifuged at 14,000 *g* (4°C for 20 min). Protein concentrations in sample supernatants were determined using RC-DC protein assay kit (Bio-Rad, USA).

2.2 | Protein digestion

Protein digestion was performed using Filter-Aided Sample Preparation (FASP) method. Fifty micrograms of protein per sample was transferred to the Microcon filter device, cut-off 30 kDa (Millipore, Germany) containing 200 μL of 8 M urea dissolved in 0.5 M TEAB, pH 8.5. Samples were centrifuged at 14,000 *g* and 20°C for 15 min. One hundred microliters of 8 M urea in 0.5 M TEAB, pH 8.5, and 10 μL of 50 mM tris (2-carboxyethyl) phosphine were added to the filter, samples were reduced on a thermomixer at 600 rpm and 37°C for 60 min and centrifuged at 14,000 *g* and 20°C for 15 min. One hundred microliters of 8 M urea in 0.5 M TEAB, pH 8.5, and 5 μL of 200 mM methyl methanethiosulfonate were added to samples in the next step. Samples were alkylated on a thermomixer at 600 rpm and 25°C for 1 min, stored without stirring in the dark for 20 min and centrifuged at 14,000 *g* and 20°C for 15 min. Subsequently, 100 μL of 0.5 M TEAB was added to the filter and samples were centrifuged at 14,000 *g* and 20°C for 20 min; this step was then repeated. Enzymatic digestion of proteins was initiated by addition of 100 μL of 0.5 M TEAB and 1.67 μL of 1 μg/μL trypsin solution (Promega, USA) dissolved in 50 mM acetic acid (trypsin ratio: cleaved protein was 1:30). Samples were mixed on thermomixer at 600 rpm and 37°C for 1 min and digested overnight at 37°C without shaking. On the next day, peptides were eluted by centrifugation at 14,000 *g* and 20°C for 15 min. Eluted peptides were desalted using C18 Silica MicroSpin columns (NestGroup Inc., USA) as previously described [22], dried under vacuum and stored at −20°C.

2.3 | LC-MS/MS analysis in DIA mode

LC-MS/MS analyses of all peptides were done using nanoElute system (Bruker, USA) connected to timsTOF Pro spectrometer (Bruker, USA). One column (no trapping column; separation column: Aurora C18, 75 μm ID, 250 mm long, 1.6 μm particles, Ion Opticks) mode was used on nanoElute system with default equilibration and sample loading conditions (separation column equilibration: 4 column volumes at 800 bars; sample loading at 800 bars using 2x pick up volume + 2 μL). Concentrated peptides were eluted by 120 min linear gradient program (flow rate 300 nL/min, 3%–30% of mobile phase B; mobile phase A: 0.1% FA in water; mobile phase B: 0.1% FA in acetonitrile) followed by system wash step at 80% mobile phase B. The analytical column was placed inside the Column Toaster (40°C; Bruker) and its emitter side was installed into CaptiveSpray ion source (Bruker, USA).

MSn data were acquired in DIA and using PASEF approach (dia-PASEF) with base method m/z range of 100–1700 and 1/k0 range of 0.6–1.6 V × s × cm^{-2}. Table S1 defines m/z 400–1100 precursor range with equal windows size of 26 Th (incl. 1 Th overlaps) using two steps each PASEF scan and cycle time of 100ms locked to 100% duty cycle.

2.4 | Processing of LC-MS/MS data by directDIA

Quantitative analysis of the LC-MS/MS DIA data was performed in Spectronaut 15.1 (Biognosys, Switzerland) software using the directDIA approach against *Mus musculus* UniProt/SwissProt database (2021_03, 17,519 sequences, downloaded on 7/29/2021). Precursor Qvalue cutoff and experiment protein Qvalue cutoff were set to 0.01. Peptides identified with *Q*-value <0.01 in at least 1 of 8 analyses were included (*q* value percentile 0.125 setting). Fixed modifications were set to Methylthio (C), variable modifications were set to Acetyl (Protein N-term) and Oxidation (M). Other parameters were set as default. Differential abundance testing was performed using Student's *t*-test in Spectronaut 15.1, proteins with absolute log2 fold change (|log2FC|) > 0.58 and with *Q*-value <0.05 were considered differentially abundant between sample groups.

2.5 | Statistical analysis

The Pearson correlation analysis and visualization of the correlation plots and was performed using GraphPad Prism (version 9.4.1).

2.6 | Gene set enrichment analysis

Gene set enrichment analysis (GSEA) in GSEA Java desktop application [23] version 4.1.0 was conducted using the list of all quantified proteins pre-ranked according to the negative log2 of the *q* value and the sign of the log2 fold change to identify enriched pathways, with a priori defined pathways from the GSKB mouse database [24]. Minimal size of a gene set was adjusted to 2, otherwise default settings were used.

The GSEA analysis was performed also using the WEB-based GEne SeT AnaLysis Toolkit (WebGestalt, http://www.webgestalt.org/) [25] Organism of interest was set to Mus musculus and Method of interest to GSEA. Analysis was performed against Gene Ontology Biological Process (GOBP) database with minimum number of genes for a category set to 3 and with FDR significance level 0.05.

2.7 | Enrichment analysis of molecular pathways

UniProt ID lists of proteins that were either statistically (*q* value <0.05) significantly up-regulated (log2FC>0.58) or down-regulated (log2FC←0.58) were separately submitted to pathway enrichment analysis using g:Profiler tool [26] that implements Fisher exact test

and multiple-test correction to evaluate pathway enrichment. Protein lists were added as ordered query sorted by the log2FC in descending manner for upregulated proteins and in ascending manner for downregulated proteins. Organism of interest was set to *Mus musculus*. Pathways from GOBP, Gene Ontology Molecular Function (GOMF), and Gene Ontology Cellular Compartment (GOCC) databases were included. Electronic GO annotations were excluded. Minimal pathway size was set to 2, maximum was set to 1000.

2.8 | Reactomes analysis

Significantly differentially expressed protein groups (q value <0.05, (|log2FC|) >0.58) were analyzed by MouseMine warehouse [27]. Obtained pathway enrichment of Reactome pathways [28] was visualized using Cytoscape [29] and Cytoscape plugins ClueGO [30] and CluePedia [31].

2.9 | Caspase-9 activity assay

Caspase-9 activity was measured by luminescence using Caspase-Glo® 9 Assay (Promega). Cell suspension (approximately 200,000 cells) was mixed with 100 μL Caspase-Glo 9 Reagent containing Caspase-Glo 9 Substrate. Cells were incubated for 2 h in the dark at 37°C. For each sample ($n = 6$), caspase-9 activity was measured in parallel in the control group and the group to which the caspase-9 inhibitor was added. Luminescence was measured by Synergy HT Microplate Reader (BioTek). The statistical significance of the difference was estimated by paired t-test.

2.10 | Staining of micromass cultures and proliferation detection

Micromass cultures grown on culture glass were fixed by 4% PFA. Alcian blue and eosin staining was used for visualisation of micromass structure and differentitation.

Cell proliferation was detected by BrdU incorporation. BrdU (B23151, Thermo Fisher Scientific) was added to culturing medium to make a 10 μM labelling solution. After two hours of incubation, cells were fixed by 4% paraformaldehyde (15 min/RT), treated by 0.1% triton X (10 min/RT) and then by HCl (0.1 M/10 min/ice; 0.2 M/10 min/RT). Cells were incubated with primary BrdU Monoclonal Antibody (MA3-071, Thermo Fisher Scientific) (1:50/overnight/4°C). BrdU-positive nuclei were visualized by Alexa Fluor® 488 (A11034 Thermo Fisher Scientific), diluted at 1:200, all nuclei were detected by ProLong® Gold Antifade reagent with DAPI (Thermo Fisher Scientific). Three repetitions were performed; frequency of BrdU-positive cells was determined in 4 different areas in the outer part of micromass culture in each repetition by Image J software analysis. More than 18,000 cells were evaluated in total.

3 | RESULTS

3.1 | Specific inhibitor effectively inhibits caspase-9 activity

To confirm the effect of Caspase-9 Inhibitor Z-LEHD-FMK, caspase-9 activity was measured by luminescence using specific caspase-9 substrate. After 2 h of incubation with caspase-9 inhibitor, activity of caspase-9 was significantly (p value <0.001) decreased (Figure 1A).

3.2 | Inhibition of caspase-9 affects structure of micromass cultures

After one week of culturing, micromass cultures develop complex microenvironment for chondrogenesis in vitro (Figure 1B). The central part of micromass spot contains predominantly differentiated chondrocytes creating 3D nodules surrounded by chondroblasts and chondrogenic precursors. The outer part of micromass spot is composed of less differentiated cells, prevalently fibroblasts. Complexity of micromass culture is supported by the presence of some smaller portion of myoblasts and tenoblasts [32].

Caspase-9 inhibition significantly affects micromass differentiation and structure. After 3 days of inhibition, micromass spots were smaller compared to control (Figure 1C,D). Inhibited micromasses developed chondrogenic nodules, but their number and area were reduced. After 6 days of caspase-9 inhibition, the differences were even more significant. Inhibited cultures showed reduced central part with differentiated nodules, whereas outer part of culture almost disappeared (Figure 1E,F).

Cell proliferation was detected by BrdU incorporation. Caspase-9 inhibition resulted in significantly decreased proliferation (Figure 1G,I) of the outer part of micromass cultures compared to control cultures (Figure 1H).

3.3 | Caspase-9 inhibition affects protein abundance in micromass cultures

To identify proteins that could be associated with caspase-9 inhibition in micromass cells, proteome changes in inhibited cells were compared to control cells treated with DMSO (inhibitor dissolvent), each condition in four biological replicates. Proteins were digested with trypsin and identified and quantified using LC-MS/MS analysis on timsTOF Pro in diaPASEF mode. In total, 7849 protein groups represented by 129,651 precursors and 94,328 peptides were quantified using Spectronaut software (FDR <0.01, Table S2). To compare this proteomics approach to other relevant methods, we labeled the same samples by 8-plex iTRAQ followed by high pH reverse phase LC fractionation and LC-MS^3 analysis on Orbitrap Lumos LC-MS system (Supplementary Methods). Using this approach, we quantified 5146 protein groups and 37,740 peptides (FDR <0.01, Table S3). Further, we re-analyzed the

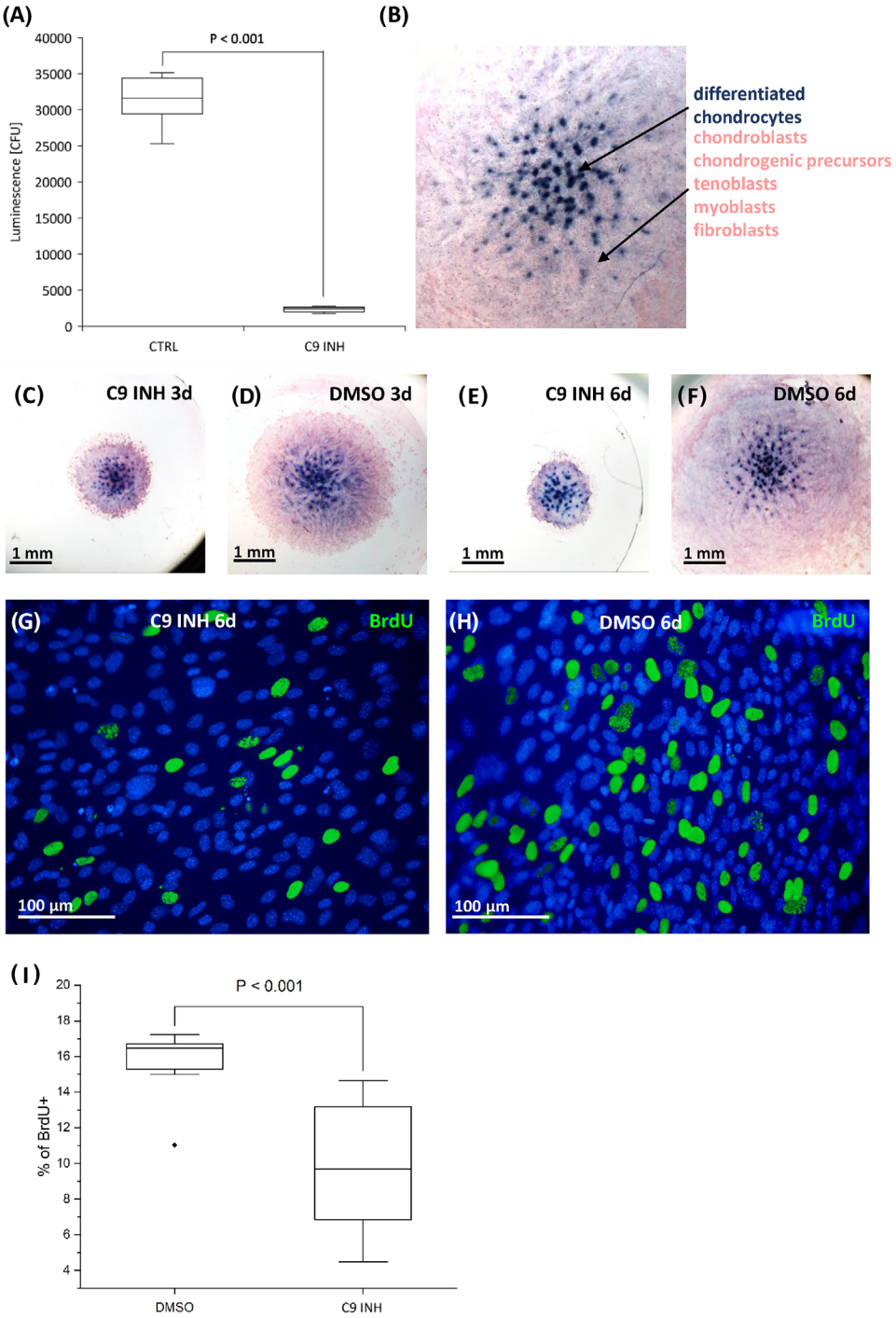

FIGURE 1 Inhibition of caspase-9 in micromass cultures. Luminescence of control (CTRL) and micromass cells treated with caspase 9 inhibitor (C9 INH) (A). Boxes show first and third quartiles, horizontal lines medians, and whiskers extreme values from six replicates. The statistical significance of the difference was estimated by paired *t*-test. Morphology of micromass cultures after caspase-9 inhibition (B–F). Micromass culture (spot) after one week of cultivation (B) showing central part with differentiated nodules (blue) and presence of different cell types according Butterfield et al. [32]. Micromass culture after 3 days of caspase-9 inhibition (C) compared to control (DMSO) cells (D). Micromass culture after 6 days of caspase-9 inhibition (E) compared to control (DMSO) cells (F). Cultures stained by alcian blue/eosin. Scale bar: 1 mm (C-F). Proliferation of the outer part of micromass culture after 6 days of caspase-9 inhibition (G) compared to controls (H). Nuclei of proliferating cells with incorporated BrdU in green, all nuclei counterstained by DAPI (blue), scale bar: 100 μm. Percentage of BrdU-positive (BrdU+) cells (I) in the outer parts of micromass cultures after 6 days of caspase-9 inhibition compared to control cultures (DMSO). Three repetitions were performed; 4 areas were counted in each repetition. The results were statistically evaluated by Mann-Whitney test, $p < 0.0001$. Results are shown in boxes (25–75 percentile), with horizontal lines showing medians and whiskers showing min-max (excluding outliers) from replicates.

same samples as for diaPASEF by conventional LC-DIA-MS on Orbitrap Lumos (Supplementary Methods, Table S1). This led to quantification of 4098 protein groups, 46,954 precursors and 35,556 peptides (FDR <0.01, Table S4). A total of 3692 protein groups and 21,093 peptides were consistently quantified by all three approaches at FDR <0.01 (Figure 2A,B). However, 2494 protein groups and 52,301 peptides were quantified exclusively by the diaPASEF method (Figure 2A,B). Comparison of quantities of protein groups specific for diaPASEF dataset and protein groups quantified also by iTRAQ 2DLC-MS3 and conventional DIA clearly show the ability of diaPASEF to analyze low abundant proteins elusive for the other two methods, due to the increased sensitivity by ion mobility spectrometry (Figure 2C). We next assessed the level of correlation between quantification by diaPASEF, iTRAQ 2DLC-MS3 and conventional DIA using the log2 fold change values of 3692 protein groups quantified by all three approaches. Comparison between diaPASEF and iTRAQ 2DLC-MS3 and diaPASEF and conventional DIA resulted in significant positive correlation in both comparisons (p value <0.0001), however the conventional DIA showed better correlation with diaPASEF (Pearson r = 0. 8293, Figure 2D) than iTRAQ 2DLC-MS3 (Pearson r = 0. 7527, Figure 2E). This leads to conclusion that although iTRAQ 2DLC-MS3 approach offers better sensitivity than conventional DIA represented by larger number of identifications, conventional DIA reaches more consistent quantification with diaPASEF. The analyzes of individual samples using both diaPASEF and conventional DIA samples display minimal variability of total intensities (Figure 2F,G) and the median of datapoints per peak varied from 7.2 to 7.9 (Figure 2H,I). Nevertheless, the Principal component analysis revealed a clear separation of micromass cells with inhibited caspase-9 and controls for all three approaches (Figure 2J–L).

Our results clearly indicate that diaPASEF method offers a superior proteome coverage compared to the iTRAQ and conventional DIA based approaches using the Orbitrap instrument. Moreover, the caspase-9 protein, whose inhibition is object of this study, was quantified only by the diaPASEF method and is missing in the iTRAQ-2DLC-MS3 and conventional DIA datasets. Thus, we proceeded with diaPASEF results for further evaluating the caspase-9 inhibition in micromass cells.

Although protein levels of caspase-9 were not influenced by the inhibitor (log2FC = 0.23, q value = 0.046) according to our criteria, effects of the caspase-9 inhibitor treatment of the cells were observed through significant (q value <0.05) upregulation (log2FC >0.58) and downregulation (log2 FC <-0.58) of 551 and 236 proteins, respectively. The heatmap (Figure 3A) visualizes precise clustering of individual biological replicates according to the caspase-9 inhibition condition.

The most significantly upregulated proteins included Ssr3, Mpeg1, Ca3, Mgst1, Scnm1, Igdcc4, Dhrs9, Scarb1, Lyz2, and Lgals2 (Table 1). These proteins could be negatively associated with caspase-9 functions. The most significantly downregulated proteins after caspase-9 inhibition represent proteins Acp5, Hbb-y, Ca9, Trim72, Atp6v0d2, Tnnc1, Mmp9, Tnni1, Tnnt1, and Myh7 (Table 1). These results represent a panel of proteins that could be associated with caspase-9 activity. All significantly downregulated and upregulated proteins are listed in Table S5.

On the other hand, from the 7 caspases quantified in our experiment, only caspase-12 showed decreased protein levels, abundances of other caspases were not affected by the caspase-9 inhibition (Table 2). Thus, we did not identify any compensatory mechanism based on elevated expression of other caspases after inhibition of caspase-9 activity in the micromass cells.

3.4 | Caspase-9 inhibition significantly affects biological pathways in primary chondrogenic cultures

To cover the biological pathways affected by caspase-9 inhibition, identified proteins were used to perform several in silico enrichment and Reactome analyses.

The GSEA analysis against the GSKB mouse database revealed association between caspase-9 inhibition and statistically significant (FDR q value <0.05) positive enrichment (NES >0) of 4 pathways in micromass cells (Figure 3B, Table S6). These molecular pathways are involved mainly in cellular detoxification. Proteins downregulated after caspase-9 inhibition represent 11 significantly negatively enriched pathways (FDR q value <0.05, NES <0) (Figure 3B, Table S6). These pathways play a role predominantly in glucose metabolism and aerobic respiration suggesting the caspase-9 inhibition to influence cellular energy metabolism.

GSEA analysis against the GOBP database using the WebGestalt tool showed positive enrichment (FDR q value <0.05, NES >0) of three pathways (Figure 3C, Table S6) after caspase-9 inhibition in micromass cells. These molecular pathways participate in lipid metabolism. Proteins downregulated after caspase-9 inhibition represent 26 (Figure 3C, Table S6) significantly negatively enriched pathways (FDR q value <0.05, NES <0). These pathways are involved in various processes including cell aggregation or collagen and muscle-related processes.

Enrichment analysis of GOBP, GOMF, and GOCC terms using the g:Profiler tool for the proteins upregulated after caspase-9 inhibition resulted in significant (adjusted p value <0.05) enrichment of 61 GOBP, 19 GOCC, and 25 GOMF pathways. The enriched pathways play a role primarily in lipid metabolism, hemostasis, and cell migration (Table S6), in agreement with the GSEA results. Proteins downregulated after caspase-9 inhibition represent 69 GOBP, 19 GOCC, and 15 GOMF pathways, majority of those involved in muscle-related processes (Table S6).

For Reactome analysis, the cut-off used for the comparison was q value <0.05 and (|log2FC|) >0.58. Networks displaying impacted pathways are shown in Figure 4A,B. In the case of upregulated proteins after caspase-9 inhibition, the affected reactome pathways included platelet degranulation, neutrophil degranulation or formation of cornified envelope (Figure 4A). The impact on the extracellular matrix organization, gluconeogenesis, and muscle contraction was apparent in downregulated proteins (Figure 4B).

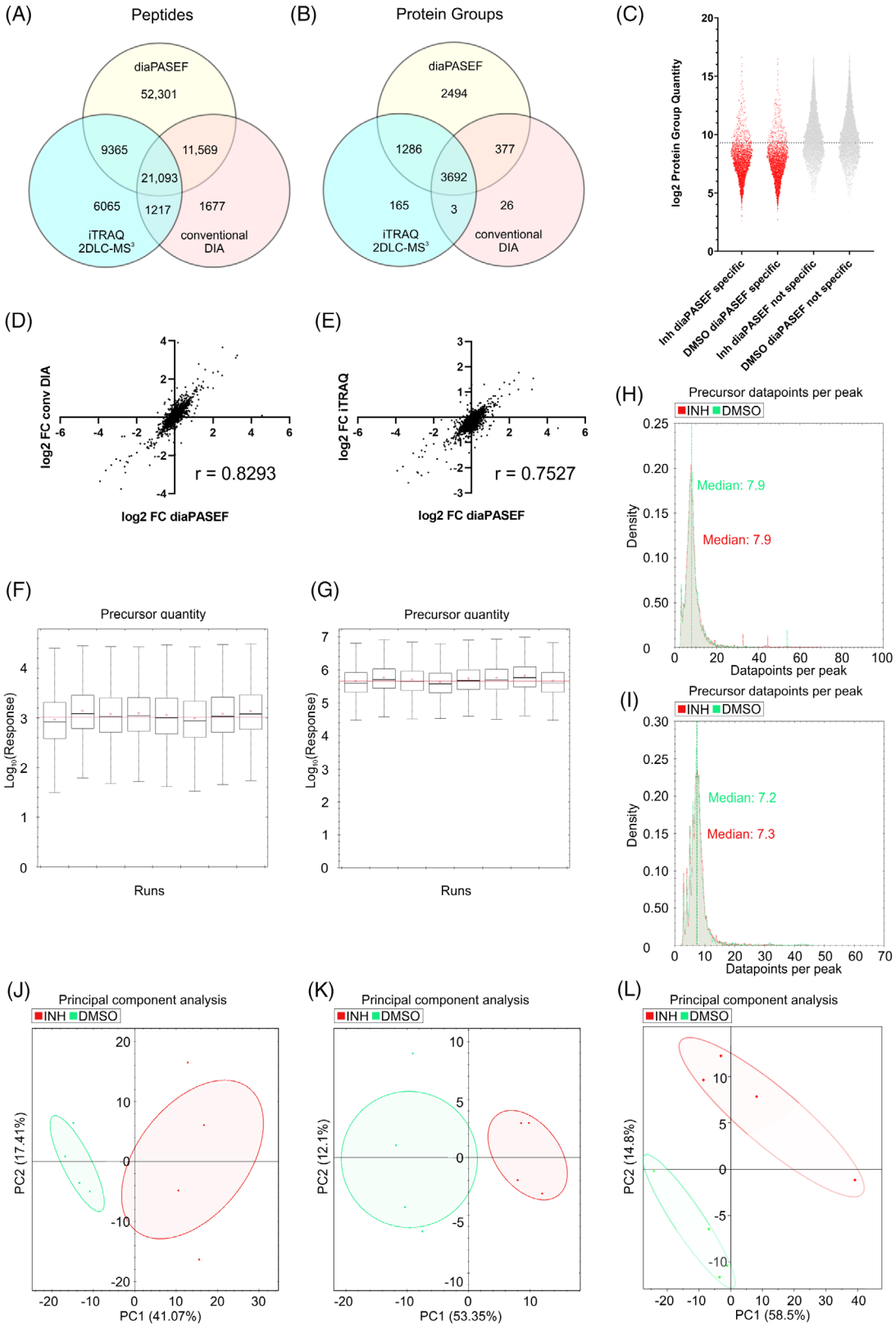

FIGURE 2 Comparison of the diaPASEF, iTRAQ-2DLC-MS3 and conventional DIA methods. Numbers of quantified (A) peptides and (B) proteins across the three LC-MS/MS approaches. (C) Comparison of quantities of proteins specific for diaPASEF dataset (red) and proteins quantified also by iTRAQ-2DLC-MS3 and conventional DIA (gray). Correlation analysis of protein log2 fold change values obtained by (D) diaPASEF and conventional DIA, and (E) by diaPASEF and iTRAQ-2DLC-MS3. Unnormalized total precursor quantity for samples analyzed using (F) diaPASEF and (G) conventional DIA. Number of datapoints per precursor peak (H) for diaPASEF and (I) for conventional DIA. Principal component analysis of protein profiles between caspase-9 inhibited and control (DMSO) samples for (J) diaPASEF, (K) conventional DIA and (L) iTRAQ-2DLC-MS3.

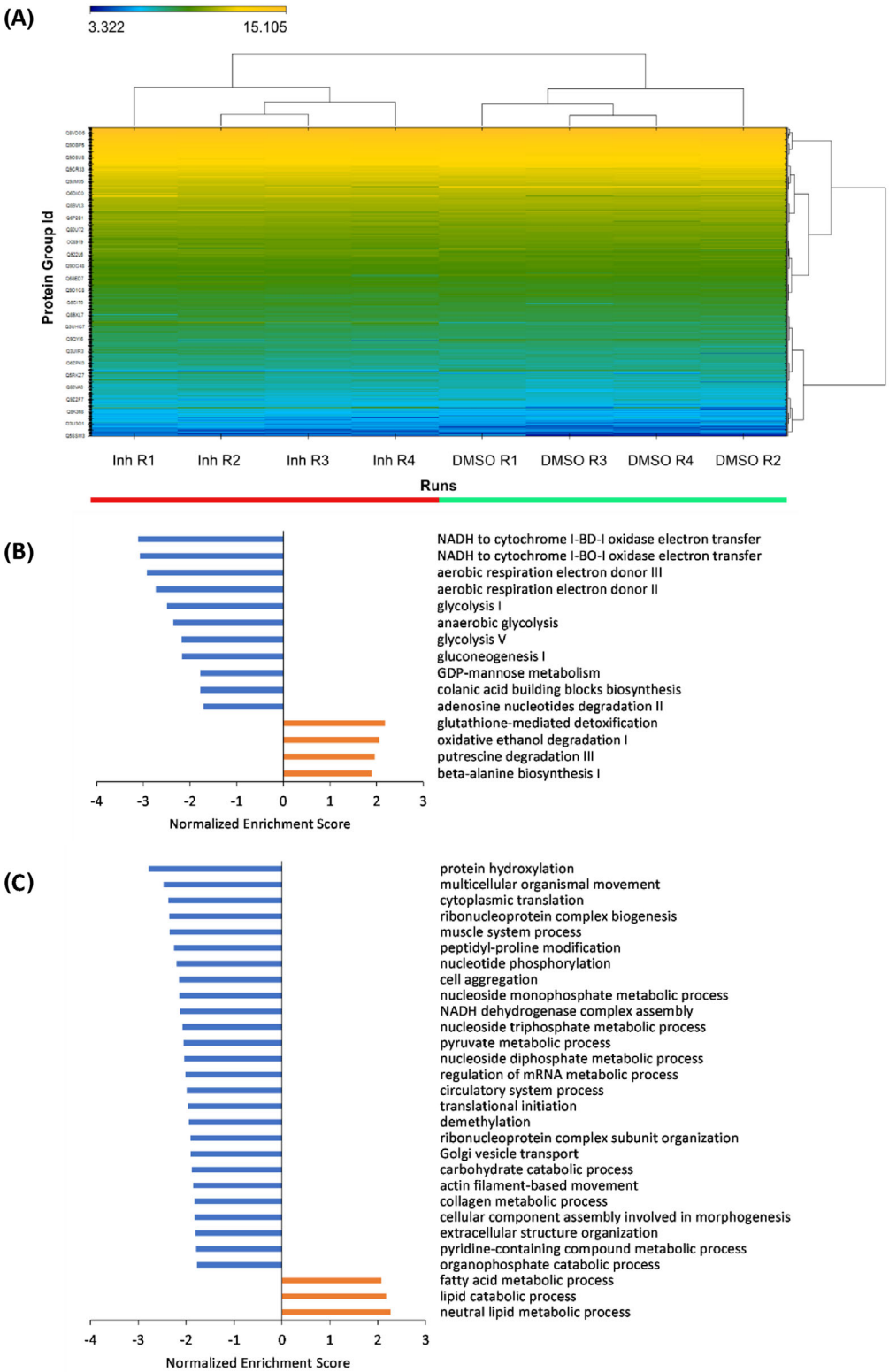

FIGURE 3 FIGURE 3 Heatmap of biological replicate clustering for micromass cells treated with caspase-9 inhibitor and control cells treated with DMSO according to the sample protein profile (A). Significantly enriched GSKB mouse pathways in GSEA analysis (B). Significantly enriched Gene Ontology Biological Process pathways in WebGestalt GSEA analysis (C).

TABLE 1 List of 30 most upregulated and downregulated proteins (according to log2FC) after caspase-9 inhibition in micromass cultures.

UniProt ID	Gene	Protein description	log2FC	*q* value
Q9DCF9	Ssr3	Translocon-associated protein subunit gamma	4.56	0.002
A1L314	Mpeg1	Macrophage-expressed gene 1 protein	3.90	2.81E-06
P16015	Ca3	Carbonic anhydrase 3	3.27	2.82E-04
Q91VS7	Mgst1	Microsomal glutathione S-transferase 1	3.19	0.001
Q8K136	Scnm1	Sodium channel modifier 1	3.04	0.011
Q9EQS9	Igdcc4	Immunoglobulin superfamily DCC subclass member 4	2.98	0.001
Q58NB6	Dhrs9	Dehydrogenase/reductase SDR family member 9	2.94	5.65E-07
Q61009	Scarb1	Scavenger receptor class B member 1	2.93	0.001
P08905	Lyz2	Lysozyme C-2	2.84	1.00E-06
Q9CQW5	Lgals2	Galectin-2	2.80	0.002
P70669	Phex	Phosphate-regulating neutral endopeptidase PHEX	2.79	2.80E-04
P97321	Fap	Prolyl endopeptidase FAP	2.51	3.35E-05
Q99P91	Gpnmb	Transmembrane glycoprotein NMB	2.50	9.82E-08
Q62283	Tspan7	Tetraspanin-7	2.49	0.010
P13707	Gpd1	Glycerol-3-phosphate dehydrogenase [NAD(+)], cytoplasmic	2.48	4.33E-04
Q6IME9	Krt72	Keratin, type II cytoskeletal 72	2.46	7.97E-06
Q3U155	Ccdc174	Coiled-coil domain-containing protein 174	2.38	6.53E-06
D3Z5L6	Slc18b1	MFS-type transporter SLC18B1	2.38	0.002
P04117	Fabp4	Fatty acid-binding protein, adipocyte	2.26	1.85E-04
Q9JHH6	Cpb2	Carboxypeptidase B2	2.24	2.35E-04
Q8R4Y4	Stab1	Stabilin-1	2.22	0.002
O54965	Rnf13	E3 ubiquitin-protein ligase RNF13	2.18	1.65E-04
Q9D8U2	Tmem41a	Transmembrane protein 41A	2.16	3.35E-05
P47750	Tshr	Thyrotropin receptor	2.16	7.91E-06
Q8VED5	Krt79	Keratin, type II cytoskeletal 79	2.11	1.14E-06
Q8VC04	Tmem106a	Transmembrane protein 106A	2.04	6.13E-07
Q8BPB5	Efemp1	EGF-containing fibulin-like extracellular matrix protein 1	2.02	1.49E-04
P56477	Irf5	Interferon regulatory factor 5	2.01	3.48E-06
P24472	Gsta4	Glutathione S-transferase A4	2.01	5.65E-07
Q8CGN5	Plin1	Perilipin-1	2.00	3.73E-04
Q05117	Acp5	Tartrate-resistant acid phosphatase type 5	-3.92	1.43E-05
P02104	Hbb-y	Hemoglobin subunit epsilon-Y2	-3.62	0.001
Q8VHB5	Ca9	Carbonic anhydrase 9	-3.33	1.78E-06
Q1XH17	Trim72	Tripartite motif-containing protein 72	-3.07	8.48E-05
Q80SY3	Atp6v0d2	V-type proton ATPase subunit d 2	-3.02	4.65E-06
P19123	Tnnc1	Troponin C, slow skeletal and cardiac muscles	-2.86	5.15E-05
P41245	Mmp9	Matrix metalloproteinase-9	-2.83	2.82E-04
Q9WUZ5	Tnni1	Troponin I, slow skeletal muscle	-2.82	7.55E-05
O88346	Tnnt1	Troponin T, slow skeletal muscle	-2.78	6.25E-05
Q91Z83	Myh7	Myosin-7	-2.77	9.92E-05
Q99PR8	Hspb2	Heat shock protein beta-2	-2.70	4.96E-05
P70402	Mybph	Myosin-binding protein H	-2.68	8.42E-05
P06467	Hbz	Hemoglobin subunit zeta	-2.64	0.001
Q7TQ48	Srl	Sarcalumenin	-2.63	4.84E-05

(Continues)

TABLE 1 (Continued)

UniProt ID	Gene	Protein description	log2FC	*q* value
P04444	Hbb-bh1	Hemoglobin subunit beta-H1	-2.61	0.001
P05977	Myl1	Myosin light chain 1/3, skeletal muscle isoform	-2.59	4.34E-05
P40935	Pnmt	Phenylethanolamine N-methyltransferase	-2.55	6.83E-05
Q38HM4;	Trim63;	E3 ubiquitin-protein ligase TRIM63;		
Q9ERP3	Trim54	Tripartite motif-containing protein 54	-2.55	2.24E-05
P09541	Myl4	Myosin light chain 4	-2.53	2.87E-05
Q8BWB1	Synpo2l	Synaptopodin 2-like protein	-2.46	9.00E-05
P97457	Mylpf	Myosin regulatory light chain 2, skeletal muscle isoform	-2.46	1.64E-05
A2AAJ9	Obscn	Obscurin	-2.44	1.48E-04
P04247	Mb	Myoglobin	-2.39	1.72E-05
P13541	Myh3	Myosin-3	-2.38	2.20E-05
A2AUC9	Klhl41	Kelch-like protein 41	-2.35	4.53E-05
P57787	Slc16a3	Monocarboxylate transporter 4	-2.35	8.10E-06
P50752	Tnnt2	Troponin T, cardiac muscle	-2.28	1.06E-04
Q9WU81	Slc37a2	Glucose-6-phosphate exchanger SLC37A2	-2.22	2.77E-04
Q9QZ47	Tnnt3	Troponin T, fast skeletal muscle	-2.17	1.23E-05
Q4FZG9	Ndufa4l2	NADH dehydrogenase [ubiquinone] 1 alpha subcomplex subunit 4-like 2	-2.15	3.60E-06

TABLE 2 Changes of abundance of 7 quantified caspase proteins after caspase-9 inhibition in the diaPASEF experiment.

UniProt ID	Gene	Protein Description	log2FC	*q* value
P29594	Casp2	Caspase-2	0.10	0.063
P70677	Casp3	Caspase-3	-0.12	4.46E-04
O08738	Casp6	Caspase-6	0.06	0.059
P97864	Casp7	Caspase-7	0.14	0.033
O89110	Casp8	Caspase-8	-0.12	0.005
Q8C3Q9	Casp9	Caspase-9	0.23	0.046
O08736	Casp12	Caspase-12	-0.63	3.31E-04

4 | DISCUSSION

Increasing body of recent studies provides evidence about yet unexpected contribution of the apoptotic caspases to proliferation and differentiation of cells [15, 33]. Recently, caspases were even assigned as a key switch between life and death [34].

Micromass cultures prepared from limb buds (autopodium) allow for work with population of chondrogenic progenitor cells and represent a traditional and well established model to investigate endochondral ossification in vitro resembling cell interactions in vivo [35]. As such, the micromass complex includes not only chondrogenic precursors, chondroblasts and chondrocytes, but also of fibroblasts, tenoblasts and myoblasts organized in concentric nodular structure upon cultivation [32]. Specific FMK-based caspase-9 inhibitor can effectively reduce caspase-9 activity in this type of cells, as confirmed by luminescence results.

The presented proteomics analysis was designed to search for the molecular background of changed formation within micromass cultures after caspase-9 inhibition which cannot be explained by decreased apoptosis as would be expected based on the traditional pro-apoptotic function of caspase-9. We applied a recent timsTOF technology [36]. offering increased sensitivity based on the implemented ion mobility separation dimension. We performed the analyzes in diaPASEF mode combining high reproducibility of DIA and sensitivity of TIMS [21]. The additional TIMS precursor separation dimension in the diaPASEF surpassed the iTRAQ-MS3 based and conventional DIA strategies on Orbitrap Lumos in the proteome coverage in our study. To our knowledge, this is one of the first applications of diaPASEF in a comparative biological experiment.

The proteomics analysis revealed molecules with multiple roles which may be related to the presence of several cell types in micromass culture. Caspase-9 inhibition significantly affected proteins associ-

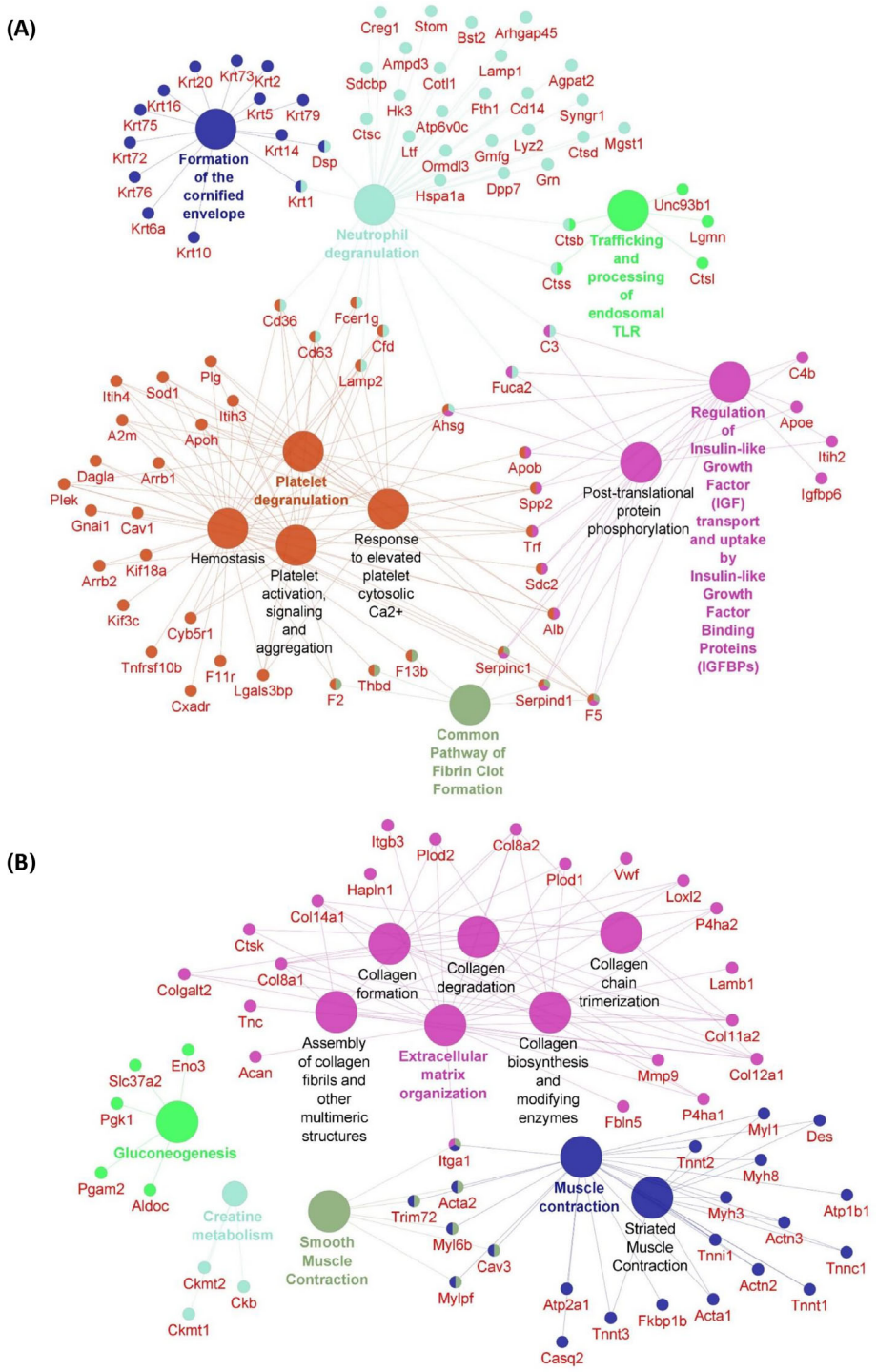

FIGURE 4 Pathways significantly enriched with up-regulated and down-regulated protein groups in micromass cells after the caspase-9 inhibitor treatment. Significantly enriched Reactome pathways [28] ($p < 0.01$) and related significantly up-regulated protein groups (q value <0.05, log2FC >0.58) in micromass cells after 6 days of caspase-9 inhibition (A). Significantly enriched Reactome pathways [28] ($p < 0.01$) and related significantly down-regulated protein groups (q value <0.05, log2FC<-0.58) in micromass cells after 6 days of caspase-9 inhibition (B).

ated with cell proliferation, tumorigenic processes, and metabolism. Altered cell proliferation after caspase-9 inhibition was subsequently confirmed by BrdU incorporation assay.

In vivo, caspase-9 is required for proper prenatal development, mainly due to its apoptotic functions [37, 38]. Caspase-9 deficiency is perinatally lethal and includes brain malformations caused by insufficient apoptotic removal. Caspase-9 inhibited micromass cultures showed significant phenotypical changes even after three days of treatment and more pronounced after 6 days. Inhibition strongly affected outer parts of micromass spots whereas chondrogenic dif-

ferentiation in central parts was affected less. Based on these observations, several possible explanations of caspase-9 effect are offered and supported by proteomics. Caspase-9 thus can play a role in proliferation, metabolism or migration of low differentiated micromass cells.

Interestingly, the most downregulated protein was tartrate-resistant acid phosphatase type 5 (PPA5). This marker of bone resorption is highly expressed in osteoclasts and chondroclasts, but PPA5 activity was also found in osteoathritic chondrocytes and as such, it was proposed as a diagnostic factor [39, 40]. The level of PPA5 was decreased after general caspase inhibition [39], in agreement with our findings which further specify the impact of caspase-9 selective inhibition.

Notably, MMP9 was found among the top ten downregulated proteins. Regulation of *Mmp9* gene expression by caspase-9 was recently described [20] in micromass cultures. Specific inhibition of caspase-9 activity caused significant decrease in *Mmp9* level, and interestingly, inhibition of MMP9 significantly decreased *Casp9* expression. This indicate an interaction between these two enzymes.

Among the 30 most decreased proteins levels in the caspase-9 inhibited group, many proteins specific for myoblast and myogenesis were found. This applies for, for example, Myosin-3, Myosin-7, Myosin light chain (MLC) 1/3, Myosin light chain 4, Myosin regulatory light chain 2, or Myosin-binding protein H. MLC1 was previously hypothesized to negatively regulate proliferation of myoblasts through inhibition of the transition from the G1 to the S phase of the cell cycle [41]. Troponin displayed downregulation at the level of all 3 components (troponin C, T, I) after caspase-9 inhibition. Troponin-T was shown to cause high levels of apoptosis in aging cells [42] and thus could be associated with the apoptotic function of caspase-9. Troponin I was reported to inhibit angiogenesis in cartilage [43] and is also able to reduce proliferation in cancer cells [44]. Notably, troponin belongs to factors being discussed in emerging roles beyond the canonical ones [45]. These findings are likely to be associated with myoblastic cells present within the micromass cultures [32] which are affected by the caspase-9 inhibition. The changes are also in agreement with previous reports showing caspase-9 to affect muscle differentiation [46].

Additionally, caspase-9 inhibited cultures showed significant decrease in many other muscle-associated proteins, for example Actin alpha, Alpha actinin-2, Calponin, or Desmin. Desmin prolonged proliferation during myogenesis in myoblasts [47] and calponin in osteoblast lineage cells lead to decreased proliferation and bone mass [48]. Myoblast differentiation is also regulated by palmdelphin [49], which was decreased after caspase-9 inhibition. Alpha actinin proteins bind actin filaments and associate with a number of cytoskeletal and signaling molecules [50]. Deregulation of cytoskeleton thus should be one mechanism of caspase-9 inhibition effect in treated cultures.

Among the top 30 upregulated proteins in caspase-9 inhibited group, several were associated with osteogenesis. One of them was osteoactivin (Gpnmb). Osteoactivin is important osteogenic regulator involved in differentiation of osteoblast and mineralization, but is highly expressed also in hypertrophic chondrocytes of growth plate [51, 52]. Others included, for example, Phex or Scarb1. Scarb1 is important for osteoblastic differentiation as shown in deficient animals [53]. Phex in abundantly expressed by osteoblasts and is involved in mineralization [54]. Recently, changes of Phex expression on RNA level were detected after caspases inhibition in osteoblastic cells [55]. Caspase-9 was previously shown to be a molecule with osteogenic potential since its inhibition caused altered expression of genes which may impact chondrogenic differentiation (Bmp4, Bmp7, Sp7, Gli1), mineral deposition (Alp, Itgam) or the remodeling of the extracellular matrix (Col1a2, Mmp9) [20].

Along with alterations in the osteogenic factors, a switch from glycolytic to lipid based metabolism was suggested by the GSEA. In cartilage, changes of lipid metabolism can lead to sever disorders such as osteoarthritis [56]. The impact of caspases in metabolism captures increasing interest in possible therapeutic applications since they apparently play roles in the pathogenesis of metabolic diseases such as obesity, the nonalcoholic steatohepatisis (NASH) and even more severe liver diseases [57]. Application of caspase inhibitors is thus a challenging approach [58]. However, one of the remaining open questions is which specific caspases have non-apoptotic roles in metabolism and related disorders [57]. The presented proteomics results indicate caspase-9 as yet another caspase participating in metabolism regulations, at least in association with chondrogenesis and endochondral osteogenesis. Despite caspase-1 and caspase-8 are of major interest in recent metabolic research, the irreversible selective inhibitor including caspase-9 (GS-9450) entered the phase-II clinical trial in patients with NASH [59]. Regional differences in chondrocyte metabolism in osteoarthritis were reported earlier [60] and caspase-9 could be one of the contributing factors.

In conclusion, inhibition of caspase-9 caused altered structural appearance of the chondrogenic micromass cultures. The proteomics analysis revealed that the changes are likely to be associated particularly with non-canonical roles of caspase-9. These novel functions included impact on proteins participating in metabolism which would thus support the novel insight into caspases as a switch between life and death [34]. Additionally, inhibition of caspase-9 modified levels of proteins having roles in cell collagen metabolic processes which would further explain the micromass morphology after caspase-9 inhibition.

Importantly, the proteomic analysis after caspase-9 inhibition indicated a metabolic switch from aerobic glycolysis to lipid based metabolism. These findings would add caspase-9 into the group of yet known caspases involved in lipid metabolism, so far consisting of caspase-1, -2, -3, -8, -11, -12 [57].

ACKNOWLEDGMENTS

The research was supported by the Czech Science Foundation (project 19-14727S). The cooperation was extended to CIISB, Instruct-CZ Centre of Instruct-ERIC EU consortium, funded by MEYS CR infrastructure project LM2023042, which is gratefully acknowledged for the financial support of the measurements at the CEITEC Proteomics Core Facility (by DP). In 2022–2023, PL was supported by the project National Institute for Cancer Research (Programme EXCELES, ID Project No. LX22NPO5102) - Funded by the European Union - Next Generation

EU. We would like to thank Ms. Kamila Rihova for her help with the analysis of cell proliferation.

CONFLICT OF INTEREST STATEMENT

The authors have declared no conflict of interest.

DATA AVAILABILITY STATEMENT

Associated Data The mass spectrometry proteomics data have been deposited to the PRIDE Archive (http://www.ebi.ac.uk/pride/archive/) via the PRIDE partner repository with the data set identifier PXD034025.

REFERENCES

1. Tsang, K. Y., & Cheah, K. S. (2019). The extended chondrocyte lineage: implications for skeletal homeostasis and disorders. *Current Opinion in Cell Biology*, *61*, 132–140.
2. Samvelyan, H. J., Madi, K., Törnqvist, A. E., Javaheri, B., & Staines, K. A. (2021). Characterisation of growth plate dynamics in murine models of osteoarthritis. *Frontiers in Endocrinology*, *12*, 734988.
3. De Luca, F. (2006). Impaired growth plate chondrogenesis in children with chronic illnesses. *Pediatric Research*, *59*, 625–629.
4. Aigner, T. (2007). Osteoarthritis. *Current opinion in rheumatology*, *19*, 427–428.
5. Van Der Kraan, P. M., & Van Den Berg, W. B. (2012). Chondrocyte hypertrophy and osteoarthritis: Role in initiation and progression of cartilage degeneration? *Osteoarthritis and Cartilage*, *20*, 223–232.
6. Tseng, C. C., Chen, Y. J., Chang, W. A., Tsai, W. C., Ou, T.-T., Wu, C.-C., Sung, W.-Y., Yen, J.-H., & Kuo, P.-L. (2020). Dual role of chondrocytes in rheumatoid arthritis: The chicken and the egg. *International Journal of Molecular Sciences*, *21*(3), 1071.
7. Chen, G. Q., Wang, S., & Hu, S. Y. (2012). Osteoporosis increases chondrocyte proliferation without a change in apoptosis during fracture healing in an ovariectomized rat model. *Molecular Medicine Reports*, *5*, 202–206.
8. Li, J., & Dong, S. (2016). The signaling pathways involved in chondrocyte differentiation and hypertrophic differentiation. *Stem Cells International*, *2016*, 2470351.
9. Kühn, K., D'lima, D. D., Hashimoto, S., & Lotz, M. (2004). Cell death in cartilage. *Osteoarthritis and Cartilage*, *12*, 1–16.
10. Chen, S., & Li, B. (2020). MiR-128-3p Post-transcriptionally inhibits WISP1 to suppress apoptosis and inflammation in human articular chondrocytes via the PI3K/AKT/NF-κB signaling pathway. *Cell Transplantation*, *29*, 963689720939131.
11. Hwang, H., & Kim, H. (2015). Chondrocyte Apoptosis in the Pathogenesis of Osteoarthritis. *International Journal of Molecular Sciences*, *16*, 26035–26054.
12. Malysheva, I. E., Topchieva, L. V., Barysheva, O. Y., Kurbatova, I. V., Vasykova, O. A., Vezikova, N. N., Marusenko, I. M., & Nemova, N. N. (2016). The level of cytokines and expression of caspase genes in rheumatoid arthritis. *Doklady. Biochemistry and Biophysics*, *468*, 226–228.
13. Musumeci, G., Castrogiovanni, P., Trovato, F., Weinberg, A., Al-Wasiyah, M., Alqahtani, M., & Mobasheri, A. (2015). Biomarkers of chondrocyte apoptosis and autophagy in osteoarthritis. *International Journal of Molecular Sciences*, *16*, 20560–20575.
14. Janečková, E., Bíliková, P., & Matalová, E. (2018). Osteogenic potential of caspases related to endochondral ossification. *The Journal of Histochemistry and Cytochemistry: Official Journal of the Histochemistry Society*, *66*, 47–58.
15. Shalini, S., Dorstyn, L., Dawar, S., & Kumar, S. (2015). Old, new and emerging functions of caspases. *Cell Death & Differentiation*, *22*, 526–539.
16. Callus, B. A., & Vaux, D. L. (2007). Caspase inhibitors: Viral, cellular and chemical. *Cell Death and Differentiation*, *14*, 73–78.
17. Adamova, E., Janeckova, E., Kleparnik, K., & Matalova, E. (2016). Caspases and osteogenic markers—in vitro screening of inhibition impact. *In Vitro Cellular & Developmental Biology - Animal*, *52*, 144–148.
18. Vesela, B., Svandova, E., Ramesova, A., Kratochvilova, A., Tucker, A. S., & Matalova, E. (2020). Caspase inhibition affects the expression of autophagy-related molecules in chondrocytes. *CARTILAGE*, *13*(2), 956S–968S.
19. Vesela, B., Zapletalova, M., Svandova, E., Ramesova, A., Doubek, J., Lesot, H., & Matalova, E. (2021). General caspase inhibition in primary chondrogenic cultures impacts their transcription profile including osteoarthritis-related factors. *Cartilage*, *13*(2), 1144S–1154S.
20. Ramesova, A., Vesela, B., Svandova, E., Lesot, H., & Matalova, E. (2022). Caspase-9 inhibition decreases expression of Mmp9 during chondrogenesis. *Histochemistry and Cell Biology*, *157*(4), 403–413.
21. Meier, F., Brunner, A. D., Frank, M., Ha, A., Bludau, I., Voytik, E., Kaspar-Schoenefeld, S., Lubeck, M., Raether, O., Bache, N., Aebersold, R., Collins, B. C., Röst, H. L., & Mann, M. (2020). diaPASEF: Parallel accumulation-serial fragmentation combined with data-independent acquisition. *Nature Methods*, *17*, 1229–1236.
22. Bouchalova, P., Sommerova, L., Potesil, D., Martisova, A., Lapcik, P., Koci, V., Scherl, A., Vonka, P., Planas-Iglesias, J., Chevet, E., Bouchal, P., & Hrstka, R. (2022). Characterization of the AGR2 interactome uncovers new players of protein disulfide isomerase network in cancer cells. *Molecular & Cellular Proteomics: MCP*, *21*, 100188.
23. Subramanian, A., Tamayo, P., Mootha, V. K., Mukherjee, S., Ebert, B. L., Gillette, M. A., Paulovich, A., Pomeroy, S. L., Golub, T. R., Lander, E. S., & Mesirov, J. P. (2005). Gene set enrichment analysis: A knowledge-based approach for interpreting genome-wide expression profiles. *Proceedings of the National Academy of Sciences of the United States of America*, *102*, 15545–15550.
24. Lai, L., Hennessey, J., Bares, V., Son, E. W., Ban, Y., Wang, W., Qi, J., Jiang, G., Liberzon, A., & Xijin Ge, S. (2016). GSKB: A gene set database for pathway analysis in mouse. *bioRxiv*, 82511.
25. Liao, Y., Wang, J., Jaehnig, E. J., Shi, Z., & Zhang, B. (2019). WebGestalt 2019: Gene set analysis toolkit with revamped UIs and APIs. *Nucleic Acids Research*, *47*, W199–W205.
26. Raudvere, U., Kolberg, L., Kuzmin, I., Arak, T., Adler, P., Peterson, H., & Vilo, J. (2019). g:Profiler: A web server for functional enrichment analysis and conversions of gene lists (2019 update). *Nucleic Acids Research*, *47*, W191–W198.
27. Motenko, H., Neuhauser, S. B., O'keefe, M., & Richardson, J. E. (2015). MouseMine: A new data warehouse for MGI. *Mammalian Genome*, *26*, 325–330.
28. Jassal, B., Matthews, L., Viteri, G., Gong, C., Lorente, P., Fabregat, A., Sidiropoulos, K., Cook, J., Gillespie, M., Haw, R., Loney, F., May, B., Milacic, M., Rothfels, K., Sevilla, C., Shamovsky, V., Shorser, S., Varusai, T., Weiser, J., … D'Eustachio, P. (2020). The reactome pathway knowledgebase. *Nucleic Acids Research*, *48*, D498–D503.
29. Shannon, P., Markiel, A., Ozier, O., Baliga, N S., Wang, J T., Ramage, D., Amin, N., Schwikowski, B., & Ideker, T. (2003). Cytoscape: A software environment for integrated models of biomolecular interaction networks. *Genome Research*, *13*, 2498–2504.
30. Bindea, G., Mlecnik, B., Hackl, H., Charoentong, P., Tosolini, M., Kirilovsky, A., Fridman, W. H., Pagès, F., Trajanoski, Z., & Galon, J. (2009). ClueGO: A Cytoscape plug-in to decipher functionally grouped gene ontology and pathway annotation networks. *Bioinformatics (Oxford, England)*, *25*, 1091–1093.
31. Bindea, G., Galon, J., & Mlecnik, B. (2013). CluePedia Cytoscape plugin: Pathway insights using integrated experimental and in silico data. *Bioinformatics (Oxford, England)*, *29*, 661–663.
32. Butterfield, N., Qian, C., & Logan, M. (2017). Pitx1 determines characteristic hindlimb morphologies in cartilage micromass culture. *PLoS ONE*, *12*(7), e0180453.

33. Nakajima, Y.-I., & Kuranaga, E. (2017). Caspase-dependent non-apoptotic processes in development. *Cell Death and Differentiation*, *24*, 1422–1430.
34. Kabigting, J. E. T., & Toyama, Y. (2020). Interplay between caspase, Yes-associated protein, and mechanics: A possible switch between life and death? *Current Opinion in Cell Biology*, *67*, 141–146.
35. Mello, M. A., & Tuan, R. S. (1999). High density micromass cultures of embryonic limb bud mesenchymal cells: An in vitro model of endochondral skeletal development. *In Vitro Cellular & Developmental Biology - Animal*, *35*, 262–269.
36. Meier, F., Brunner, A. D., Koch, S., Koch, H., Lubeck, M., Krause, M., Goedecke, N., Decker, J., Kosinski, T., Park, M. A., Bache, N., Hoerning, O., Cox, J., Räther, O., & Mann, M. (2018). Online Parallel Accumulation-Serial Fragmentation (PASEF) with a novel trapped ion mobility mass spectrometer. *Molecular & Cellular Proteomics: MCP*, *17*, 2534–2545.
37. Kuida, K., Haydar, T. F., Kuan, C.-Y., Gu, Y., Taya, C., Karasuyama, H., Su, M S.-S, Rakic, P., & Flavell, R. A. (1998). Reduced apoptosis and cytochrome c–mediated caspase activation in mice lacking caspase 9. *Cell*, *94*, 325–337.
38. Hakem, R., Hakem, A., Duncan, G. S., Henderson, J. T., Woo, M., Soengas, M. S., Elia, A., De La Pompa, J. L., Kagi, D., Khoo, W., Potter, J., Yoshida, R., Kaufman, S. A., Lowe, S. W., Penninger, J. M., & Mak, T. W. (1998). Differential requirement for caspase 9 in apoptotic pathways in vivo. *Cell*, *94*, 339–352.
39. Seol, J. W., Lee, H. B., Kim, N. S., & Park, S. Y. (2009). Tartrate-resistant acid phosphatase as a diagnostic factor for arthritis. *International Journal of Molecular Medicine*, *24*, 57–62.
40. Olszewska-Slonina, D., Jung, S., Matewski, D., Olszewski, K. J., Krzyzynska-Malinowska, E., Braszkiewicz, A., & Kowaliszyn, B. (2015). Lysosomal enzymes in serum and synovial fluid in patients with osteoarthritis. *Scandinavian Journal of Clinical and Laboratory Investigation*, *75*, 145–151.
41. Zhang, S.-Z., Xu, Y., Xie, H.-Q., Li, X. Q., Wei, Y.-Q., & Yang, Z. M. (2009). The possible role of myosin light chain in myoblast proliferation. *Biological Research*, *42*, 121–132.
42. Zhang, T., Birbrair, A., Wang, Z. M., Taylor, J., Messi, M. L., & Delbono, O. (2013). Troponin T nuclear localization and its role in aging skeletal muscle. *Age (Dordrecht, Netherlands)*, *35*, 353–370.
43. Moses, M. A., Wiederschain, D., Wu, I., Fernandez, C. A., Ghazizadeh, V., Lane, W. S., Flynn, E., Sytkowski, A., Tao, T., & Langer, R. (1999). Troponin I is present in human cartilage and inhibits angiogenesis. *Proceedings of the National Academy of Sciences of the United States of America*, *96*, 2645–2650.
44. Casas-Tintó, S., Maraver, A., Serrano, M., & Ferrús, A. (2016). Troponin-I enhances and is required for oncogenic overgrowth. *Oncotarget*, *7*, 52631–52642.
45. Johnston, J. R., Chase, P. B, & Pinto, J. R. (2018). Troponin through the looking-glass: Emerging roles beyond regulation of striated muscle contraction. *Oncotarget*, *9*, 1461–1482.
46. Murray, T. V. A., Mcmahon, J. M., Howley, B. A., Stanley, A., Ritter, T., Mohr, A., Zwacka, R., & Fearnhead, H. O. (2008). A non-apoptotic role for caspase-9 in muscle differentiation. *Journal of Cell Science*, *121*, 3786–3793.
47. Smythe, G. M., Davies, M. J., Paulin, D., & Grounds, M. D. (2001). Absence of desmin slightly prolongs myoblast proliferation and delays fusion in vivo in regenerating grafts of skeletal muscle. *Cell and Tissue Research*, *304*, 287–294.
48. Su, N., Chen, M., Chen, S., Li, C., Xie, Y., Zhu, Y., Zhang, Y., Zhao, L., He, Q., Du, X., Chen, D., & Chen, L. (2013). Overexpression of H1 calponin in osteoblast lineage cells leads to a decrease in bone mass by disrupting osteoblast function and promoting osteoclast formation. *Journal of Bone and Mineral Research : The Official Journal of the American Society for Bone and Mineral Research*, *28*, 660–671.
49. Nie, Y., Chen, H., Guo, C., Yuan, Z., Zhang, X., Mo, D., & Chen, Y. (2017). Palmdelphin promotes myoblast differentiation and muscle regeneration. *Scientific Reports*, *7*, 41608.
50. Sjöblom, B., Salmazo, A., & Djinovic-Carugo, K. (2008). Alpha-actinin structure and regulation. *Cellular and Molecular Life Sciences: CMLS*, *65*, 2688–2701.
51. Abdelmagid, S. M., Barbe, M. F., Hadjiargyrou, M., Owen, T. A., Razmpour, R., Rehman, S., Popoff, S. v. N., & Safadi, F. F. (2010). Temporal and spatial expression of osteoactivin during fracture repair. *Journal of Cellular Biochemistry*, *111*, 295–309.
52. Abdelmagid, S. M., Belcher, J. Y., Moussa, F. M., Lababidi, S. L., Sondag, G. R., Novak, K. M., Sanyurah, A. S., Frara, N. A., Razmpour, R., Del Carpio-Cano, F. E., & Safadi, F. F. (2014). Mutation in osteoactivin decreases bone formation in vivo and osteoblast differentiation in vitro. *The American Journal of Pathology*, *184*, 697–713.
53. Tourkova, I. L., Dobrowolski, S. F., Secunda, C., Zaidi, M., Papadimitriou-Olivgeri, I., Papachristou, D. J., & Blair, H. C. (2019). The high-density lipoprotein receptor Scarb1 is required for normal bone differentiation in vivo and in vitro. *Laboratory investigation; a journal of technical methods and pathology*, *99*, 1850–1860.
54. Ruchon, A. F., Tenenhouse, H. S., Marcinkiewicz, M., Siegfried, G., Aubin, J. E., Desgroseillers, L., & Boileau, G. (2000). Developmental expression and tissue distribution of Phex protein: effect of the Hyp mutation and relationship to bone markers. *Journal of Bone and Mineral Research : The Official Journal of The American Society for Bone and Mineral Research*, *15*, 1440–1450.
55. Kratochvílová, A., Veselá, B., Ledvina, V., Švandová, E., Klepárník, K., Dadáková, K., Beneš, P., & Matalová, E. (2020). Osteogenic impact of pro-apoptotic caspase inhibitors in MC3T3-E1 cells. *Scientific Reports*, *10*, 7489.
56. Gkretsi, V., Simopoulou, T., & Tsezou, A. (2011). Lipid metabolism and osteoarthritis: Lessons from atherosclerosis. *Progress in Lipid Research*, *50*, 133–140.
57. Wilson, C. H., & Kumar, S. (2018). Caspases in metabolic disease and their therapeutic potential. *Cell Death and Differentiation*, *25*, 1010–1024.
58. Dhani, S., Zhao, Y., & Zhivotovsky, B. (2021). A long way to go: Caspase inhibitors in clinical use. *Cell Death & Disease*, *12*, 949.
59. Ratziu, V. (2012). Treatment of NASH with ursodeoxycholic acid: pro. *Clinics and Research in Hepatology and Gastroenterology*, *36*(Suppl 1), S41–5.
60. Fukui, N., Ikeda, Y., Ohnuki, T., Tanaka, N., Hikita, A., Mitomi, H., Mori, T., Juji, T., Katsuragawa, Y., Yamamoto, S., Sawabe, M., Yamane, S., Suzuki, R., Sandell, L. J., & Ochi, T. (2008). Regional differences in chondrocyte metabolism in osteoarthritis: a detailed analysis by laser capture microdissection. *Arthritis and Rheumatism*, *58*, 154–163.

SUPPORTING INFORMATION

Additional supporting information may be found online https://doi.org/10.1002/pmic.202200408 in the Supporting Information section at the end of the article.

How to cite this article: Lapcik, P., Vesela, B., Potesil, D., Dadakova, K., Zapletalova, M., Benes, P., Bouchal, P., & Matalova, E. (2023). DiaPASEF proteotype analysis indicates changes in cell growth and metabolic switch induced by caspase-9 inhibition in chondrogenic cells. *Proteomics*, *23*, e2200408. https://doi.org/10.1002/pmic.202200408